

# The role of conformational flexibility in prion propagation and maintenance for Sup35p

Thomas Scheibel and Susan L. Lindquist

Howard Hughes Medical Institute and Department of Molecular Genetics and Cell Biology, University of Chicago, Chicago, Illinois 60637, USA.

**The  $[PSI^+]$  factor of *Saccharomyces cerevisiae* is a protein-based genetic element (prion) comprised of a heritable altered conformation of the cytosolic translation termination factor Sup35p. *In vitro*, the prion-determining region (NM) of Sup35p undergoes conformational conversion from a highly flexible soluble state to structured amyloid fibers, with a rate that is greatly accelerated by preformed NM fiber nuclei. Nucleated conformational conversion is the molecular basis of the genetic inheritance of  $[PSI^+]$  and provides a new model for studying amyloidogenesis. Here we investigate the importance of structure and structural flexibility in soluble NM. Elevated temperatures, chemical chaperones and certain mutations in NM increase or change its structural content and inhibit or enhance nucleated conformational conversion. We propose that the structural flexibility of NM is particularly suited to allowing heritable protein-based changes in cellular behavior.**

The  $[PSI^+]$  factor, a protein-based genetic element (prion) of *Saccharomyces cerevisiae*, represents a newly discovered type of epigenetic inheritance in which changes in phenotype are transmitted through self-perpetuating, conformationally altered forms of cellular proteins<sup>1,2</sup>. The inheritance of  $[PSI^+]$  from mother to daughter cells is based on the transmission of conformational information from ordered nonfunctional Sup35p aggregates to the soluble, functional Sup35p, a subunit of the polypeptide chain release complex that is essential for translation termination<sup>3-5</sup>. This molecular mechanism is reminiscent of the self-promoted conformational conversion proposed for mammalian prion diseases<sup>4-6</sup>, but in yeast it produces heritable changes in metabolism rather than disease. *In vitro*, the prion-determining region of Sup35, NM, has the unusual property of remaining as a random coil-rich protein in solution for hours before it converts to a structure with all the characteristics of amyloid fibers<sup>7,8</sup>. The contribution of structural content in the soluble protein prior to conformational conversion is a major

unanswered question in prion biology. Here we show that factors influencing conformational flexibility of Sup35/NM influence amyloid propagation *in vitro*. Together with other analyses *in vivo*, our data suggest that the unusual structural properties and the conformational flexibility of the NM-region of Sup35 contribute to the mechanism by which it serves as a protein-based element of genetic inheritance.

## NM purification with and without denaturant

Because NM tends to polymerize during purification, previous *in vitro* studies used protein purified in denaturant, followed by dilution into physiological buffer, to investigate conformational conversion<sup>7-9</sup>. The random coil content of such resolubilized NM is unusually high, emphasizing the importance of ensuring that the structure and behavior of NM purified under these conditions reflect that of NM unexposed to denaturant. We purified a GST-NM fusion protein under non-denaturing conditions, removed the GST domain by proteolytic cleavage and compared it to the standard NM preparation for secondary structure content, amyloid assembly kinetics and amyloid fiber morphology. NM in 8 M guanidinium chloride showed a CD spectrum indicative of a random coil with no detectable secondary structure (Fig. 1a). In physiological buffer, NM displayed a far-UV CD signal representative of a molecule rich in random coil but partially structured, regardless of whether it had been purified under denaturing or non-denaturing conditions (Fig. 1a). The rates of conformational conversion determined by Congo red (CR) binding<sup>10</sup> for both un-nucleated and nucleated reactions were indistinguishable for NM prepared under both conditions (Fig. 1b; data not shown). Fiber morphology was indistinguishable when visualized by either electron (EM) or atomic force (AFM) microscopy (data not shown; refs 7,8). More important, NM prepared under both conditions showed the same changes in behavior when exposed to elevated temperature or chemical chaperones (see below). Because these criteria detected no differences between the two types of preparation, further studies employed NM purified under denaturing conditions due to higher yields and greater ease of handling.

## Contribution of partially structured NM to conversion

Many proteins reach their final stable structures by progressing through partially folded intermediates. This is also true of amyloid polymerization, where mildly denaturing conditions, such as low pH or elevated temperatures, produce partially unfolded intermediates that provide the basis for conformational conversion<sup>11-13</sup>. To determine whether the partially structured state that naturally exists in the soluble

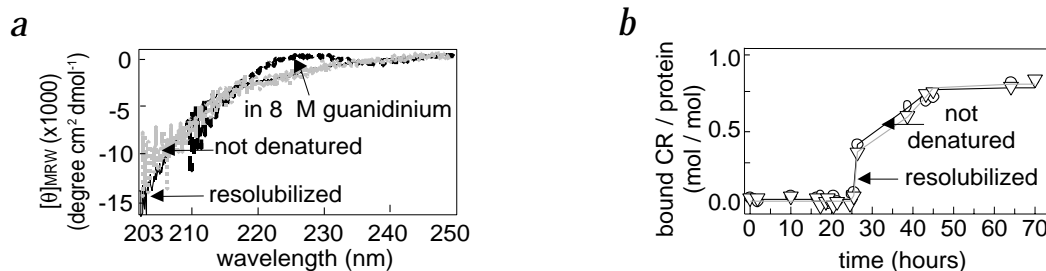


**Fig. 1** Comparison of NM<sup>wt</sup> purified under denaturing and non-denaturing conditions. **a**, Secondary structure of resolubilized NM<sup>wt</sup> (10  $\mu$ M) and non-denatured NM<sup>wt</sup> (0.5  $\mu$ M, the low concentration is due to technical difficulties in concentrating) by far-UV CD. The higher signal noise for non-denatured NM<sup>wt</sup> is due to a lower protein concentration. Shown are NM<sup>wt</sup> diluted out of denaturant (solid black line); non-denatured NM<sup>wt</sup> (dotted gray line); and NM<sup>wt</sup> in 8 M guanidinium chloride (dotted black line). **b**, Unseeded, unrotated conformational conversion of resolubilized and non-denatured protein (0.5  $\mu$ M each) was monitored by CR binding. NM<sup>wt</sup> diluted out of denaturant is represented by a circle; non-denatured NM<sup>wt</sup> by triangle.

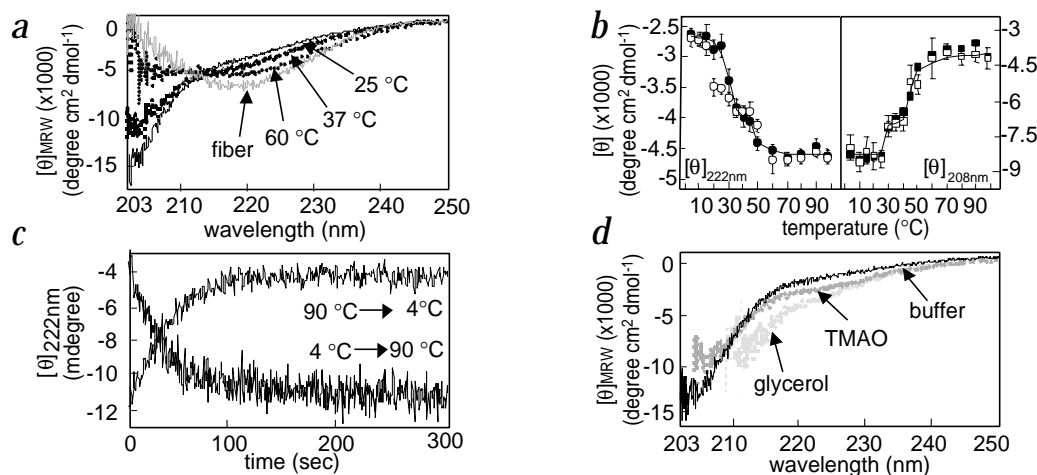


**Fig. 2** Influences of temperature and chemical chaperones on NM<sup>wt</sup> secondary structure. **a**, Temperature-induced NM<sup>wt</sup> (10  $\mu$ M) secondary structure changes by far-UV CD. NM<sup>wt</sup> remained at each temperature for 10 min before the spectrum was taken. For comparison, a far UV-CD spectrum of NM<sup>wt</sup> fibers is shown. **b**, The mean residue ellipticities of NM<sup>wt</sup> increased at  $[\theta]_{222\text{nm}}$  (filled circle) and decreased at  $[\theta]_{208\text{nm}}$  (filled square) as a function of temperature. The transition is thermodynamically reversible in a heating-cooling experiment (closed versus open symbols). **c**, Time course of temperature-induced gain (solid black line) and loss (dotted gray line) of NM<sup>wt</sup> (5  $\mu$ M) secondary structure monitored at 222 nm. The reaction is concentration-independent between 0.5  $\mu$ M and 65  $\mu$ M. NM<sup>wt</sup> was incubated at each temperature for 30 min before shifting to the final temperature. The kinetics could be fit with a single exponential, with rate constants  $k_{\text{gain}} = 1.7 \times 10^{-2} \text{ s}^{-1}$  and  $k_{\text{loss}} = 1.9 \times 10^{-2} \text{ s}^{-1}$ . **d**, NM<sup>wt</sup> secondary structure by far-UV CD. Buffer is standard buffer (solid black line); TMAO, standard buffer plus 2.5 M TMAO (dotted dark gray line); and glycerol, standard buffer plus 3 M glycerol (25 %) (dotted light gray line).

form of NM contributes to nucleated conformational conversion, we tested the effects of elevated temperatures, chemical chaperones and certain NM mutants. All of the conditions described influenced neither the quaternary structure of soluble NM nor that of assembled amyloid fibers as detected by static and dynamic light scattering or AFM (see below; data not shown).

#### Temperature-induced gain of structure

With increasing temperature, NM underwent a conformational transition from a random coil-dominated structure to one with high secondary structure content that remained distinct from that of  $\beta$ -sheet-rich amyloid fibers (Fig. 2a). The amplitude for the mean residue ellipticity at  $[\theta]_{222\text{nm}}$  (reflecting structural content) increased, whereas the amplitude for the mean residue ellipticity at  $[\theta]_{208\text{nm}}$  (reflecting random coil content) decreased. Because of the large impact of the random-coil structure on the CD signal of NM at 218 nm, which is commonly used to monitor  $\beta$ -sheet secondary structure, 222 nm was chosen as a more reliable indicator of secondary structure gain. Above 60 °C, structural content remained stable up to 98 °C (Fig. 2b; data not shown), even with prolonged incubation (90 min) (data not shown).

For proteins from mesophilic organisms, the gain of stable soluble structure with increasing temperature is very unusual because these proteins usually denature and aggregate at high temperatures<sup>14</sup>. A small number of proteins, including certain amyloidogenic polypeptides, are notable exceptions<sup>15–18</sup>. In contrast to the one other amyloidogenic peptide tested<sup>15</sup>, the temperature-induced structural gain in NM was thermodynamically reversible and exhibited no hysteresis, suggesting that it gains and loses structure through similar pathways (Fig. 2b). The rates of the structural gain and loss were kinetically indistinguishable, with rate constants of  $k_{\text{gain}} = 1.7 (\pm 0.1) \times 10^{-2} \text{ s}^{-1}$  and  $k_{\text{loss}} = 1.9 (\pm 0.1) \times 10^{-2} \text{ s}^{-1}$  (Fig. 2c). Thus, NM behavior is unique in many respects, even from other proteins with high structural flexibility.

#### Effect of osmolytes on secondary structure

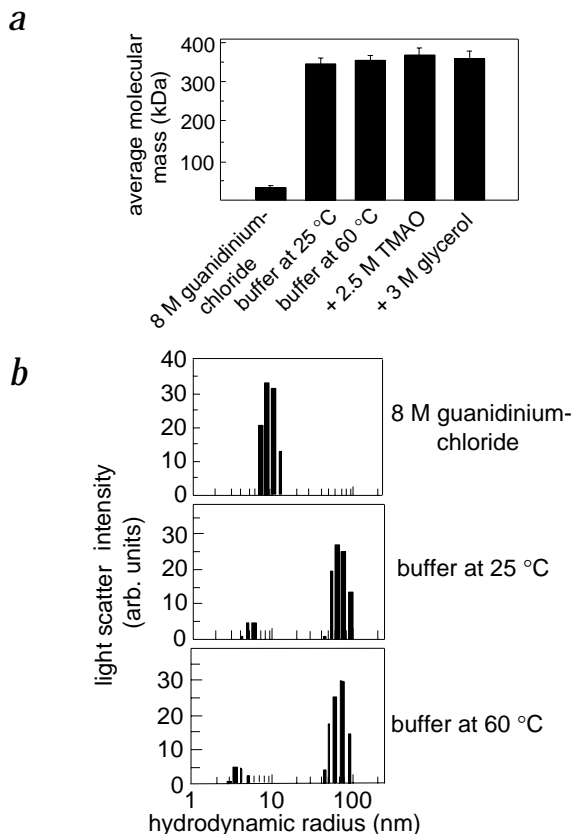
Osmolytes have been shown to accelerate conformational conversion of an amyloidogenic polypeptide<sup>19</sup>. Therefore, they may influence the partially structured state of soluble NM. Increasing trimethylamine N-oxide (TMAO) to 2.5 M or glycerol to 3 M (25% glycerol) led to a gain of NM secondary structure with no further changes at higher concentrations (Fig. 2d; data not shown). Because of the large impact of random-coil structure on the CD signal of NM, the changes appear small. However, in the presence of glycerol, the signal increased 60% and in the presence of TMAO it increased 100% at 222 nm. These effects of TMAO and glycerol were specific and not simply based on enhancing local concentrations or changes in ionic strength, because incubation with the osmolyte trehalose (3 M) or with NaCl (1 M) had no apparent influence on NM secondary structure (data not shown). Further, examination of each sample after the CD analysis by EM, AFM and CR binding confirmed that no amyloidic material was formed during the experiment.

#### Effects on quaternary structure

To determine if the quaternary structure of NM is altered by elevated temperature or osmolytes, we monitored static and dynamic light scattering. In 8 M GdmCl, the average molecular mass of monomeric NM is  $31,500 \pm 700$  Da, which is close to the calculated mass of 28,516 Da of the NM monomer (Fig. 3a). Quasi-elastic light scattering showed a hydrodynamic radius of  $9 \pm 2$  nm, reflecting a highly hydrated random coil structure (Fig. 3b). In physiological buffer, NM had an average molecular mass of  $348,900 \pm 21,400$  Da, resulting from an equilibrium between monomeric and oligomeric species (Fig. 3a,b). The influences of elevated temperature, glycerol and TMAO on the average molecular mass did not exceed the error of the measurements (Fig. 3a). Further, the oligomerization status of NM showed no concentration dependence between 0.7  $\mu$ M and 46  $\mu$ M (data not shown; ref. 8). The hydrodynamic radius of renatured monomeric NM at 25 °C was  $4 \pm 1$  nm, which shifted

## letters

**Fig. 3** Influences of temperature and chemical chaperones on NM<sup>wt</sup> (10 μM) quaternary structure. **a**, Static light scattering. The molecular mass of NM<sup>wt</sup> in 8 M GdmCl is 31,500 ± 1000 Da (calculated mass 28,516 Da); in 5mM potassium phosphate, 50 mM GdmCl and 150 mM NaCl (buffer) at 25 °C, it is 348,900 ± 21,400 Da and at 60 °C is 356,900 ± 22,400 Da; in the presence of 2.5 M TMAO, it is 367,500 ± 19,000 Da; and the molecular mass of NM<sup>wt</sup> in the presence of 3M glycerol is 360,600 ± 19,500 Da. **b**, Quasi-elastic light scattering. Denatured NM<sup>wt</sup> shows a hydrodynamic radius of 9 ± 2nm, and NM<sup>wt</sup> in buffer at 25 °C shows a hydrodynamic radius of 4 ± 1 nm for monomers and hydrodynamic radii between 50nm and 130nm for oligomers (intensity normalized). At 60 °C, the hydrodynamic radii are slightly shifted towards smaller values. In equilibrium, 87 ± 5% of the soluble protein is monomeric (mass normalized) in buffer at all temperatures.



slightly towards smaller radii at elevated temperature. Oligomers of NM had hydrodynamic radii between 50 nm and 130 nm, indicating an oligomer distribution from 10- to 30-mers (Fig. 3b). Mass-normalization of the dynamic light scattering data indicated that 87 ± 5% of NM was monomeric in equilibrium, independent of temperature (data not shown).

#### Influence of structural state on conversion

As the ability of preformed fibers to promote the conformational conversion — that is, nucleated conformational conversion — of soluble NM provides a simple molecular model for the propagation of [PSI<sup>+</sup>]<sup>7-9</sup>, we investigated the influence of the structural state of NM on this process. At 25 °C in physiological buffer, the apparent nucleated conformational conversion rate for soluble NM was  $k_{app} = 4.2 (\pm 0.2) \times 10^{-4} \text{ s}^{-1}$  in the presence of excess nuclei. Temperatures above 25 °C slowed the rate of nucleated conformational conversion, with complete inhibition above 60 °C (Fig. 4a,b). Temperature shifts confirmed thermodynamic and kinetic reversibility of this inhibition (Fig. 4c). NaCl and trehalose had no influence on the conversion rate, but TMAO and glycerol increasingly inhibited nucleated conformational conversion with increasing concentrations (Fig. 4d; data not shown). Thus, both the effects of temperature and osmolytes on nucleated conformational conversion of NM contrast with the

effects on other amyloidogenic polypeptides studied so far, where fiber assembly was accelerated under such conditions<sup>15-19</sup>.

#### Conversion of NM oligopeptide repeat mutants

The biological relevance of the structural flexibility of NM in the propagation of [PSI<sup>+</sup>] is suggested by the fact that growth on

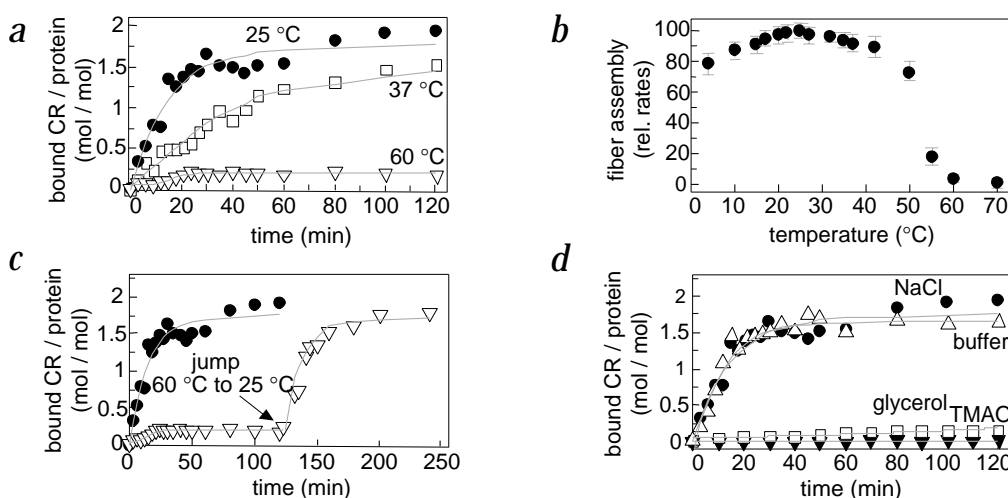


**Fig. 4** Influences of temperature and chemical chaperones on nucleated conformational conversion of NM<sup>wt</sup> (5 μM) in the presence of sonicated preformed NM<sup>wt</sup> fibers (5 % w/w) and monitored by CR binding. **a**, Influence of temperature on nucleated conformational conversion. Temperatures shown are 25 °C (open circle); 37 °C (open square); and 60 °C (open triangle). **b**, Nucleated conformational conversion rates are plotted against temperature. The nucleated conformational conversion rate ( $k_{app} = 4.2 (\pm 0.2) \times 10^{-4} \text{ s}^{-1}$ ) at 25 °C is set to 100. **c**, Soluble NM<sup>wt</sup> (5 μM) was incubated with nucleating fibers at 60 °C for 2 h before shifting to 25 °C (triangle). The nucleated conformational conversion at 25 °C is shown in comparison (filled circle). **d**, Influence of osmolytes on nucleated conformational conversion. Conditions shown are standard buffer (filled circle); standard buffer plus 1 M NaCl (open triangle); standard buffer plus 3 M glycerol (25 %) (open square); and standard buffer plus 2.5 M TMAO (filled triangle). All solid lines represent sigmoidal curve fits.

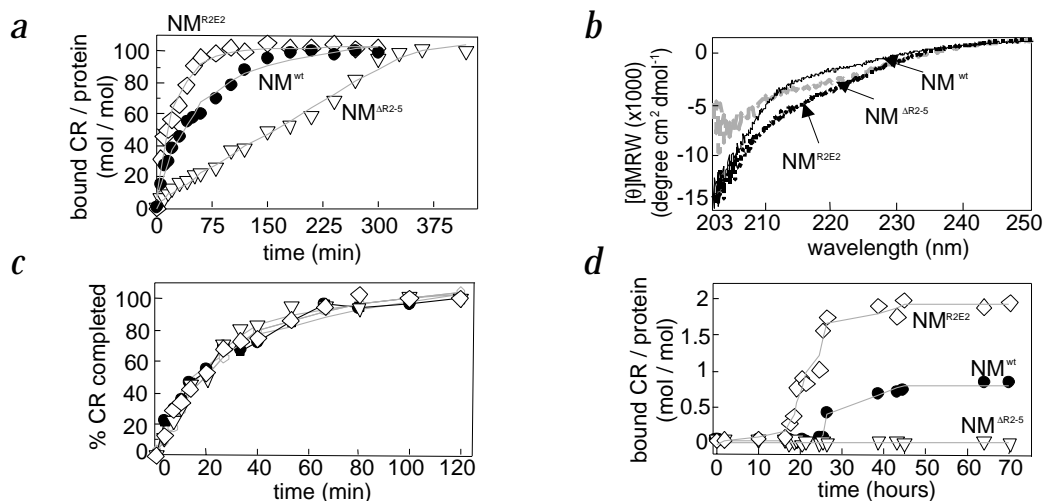


**Fig. 5** Mutations in the oligopeptide repeats of NM influence structure and conformational conversion. **a**, Nucleated conformational conversion (5  $\mu$ M each). Shown are NM<sup>wt</sup> nucleated with NM<sup>wt</sup> 5% (w/w) fibers (filled circle); NM<sup>AR2-5</sup> nucleated with NM<sup>AR2-5</sup> 5% (w/w) fibers (open triangle); and NM<sup>R2E2</sup> nucleated with NM<sup>R2E2</sup> 5% (w/w) fibers (open diamond). **b**, Far-UV CD of the secondary structure of NM<sup>wt</sup> (solid black line), NM<sup>AR2-5</sup> (dotted gray line) and NM<sup>R2E2</sup> (dotted black line) (10  $\mu$ M each). **c**, Cross-seeding of soluble NM<sup>wt</sup> (5  $\mu$ M) with 5% (w/w) each of NM<sup>wt</sup> fibers (filled circle), NM<sup>AR2-5</sup> fibers (open triangle) or NM<sup>R2E2</sup> fibers (open diamond). All solid lines represent sigmoidal curve fits. **d**, Unseeded, unrotated conformational conversion of (5  $\mu$ M each) NM<sup>wt</sup> (filled circle), NM<sup>AR2-5</sup> (open triangle) and NM<sup>R2E2</sup> (open diamond).

high concentrations of glycerol leads to the loss of  $[PSI^+]$ <sup>20</sup> (H.-C. Chang and S.L.L., unpublished results). In contrast, altering the level of trehalose, the other major osmolyte of yeast that stabilizes normal proteins in the folded state<sup>21</sup>, had little effect on  $[PSI^+]$  gain or loss (H.-C. Chang and S.L.L., unpublished results). To investigate the involvement of NM structure in the maintenance and propagation of  $[PSI^+]$  more directly, we studied the structural properties of established oligopeptide repeat mutants<sup>22</sup>.

The oligopeptide repeats of NM have five imperfect copies of a peptide with the motif PQQGYQQ-YN. These repeats constitute one of the few similarities of Sup35 to the mammalian prion protein (PrP), which has a different function and different cellular location (Sup35 is cytosolic). Reduction in the number of oligopeptide repeats reduces prion propagation, and expansion of the repeats induces their spontaneous appearance of Sup35 in yeast<sup>22</sup> and PrP in mammals<sup>6</sup>. The partial oligopeptide repeat deletion in NM (NM<sup>AR2-5</sup>) that causes loss of  $[PSI^+]$ <sup>22</sup> had a slower rate of nucleated conformational conversion than NM<sup>wt</sup> *in vitro* (Fig. 5a). NM<sup>AR2-5</sup> exhibited a less flexible structure with more secondary structure content, similar to that of wild type protein at elevated temperature or in the presence of chemical chaperones (Fig. 5b). 'Cross-seeding' experiments, where each soluble protein was nucleated with fibers derived from the other protein, demonstrated that the rates of conformational conversion did not depend upon the nuclei. Rather, the critical difference in rates depended upon the soluble state of NM (Fig 5c; data not shown).

The oligopeptide repeat expansion NM<sup>R2E2</sup>, which increases the spontaneous frequency of  $[PSI^+]$  formation<sup>22</sup>, showed a shifted CD signal compared to NM<sup>wt</sup>, indicating a significant difference in secondary structure (Fig. 5b). The far-UV CD signal changes for NM<sup>R2E2</sup> (and for NM<sup>AR2-5</sup>) could possibly be caused by changed orders of aromatic side chains. In any case, the changes of NM<sup>R2E2</sup> slightly enhanced its conformational conversion in nucleated reactions compared to NM<sup>wt</sup> (Fig. 5a). In unseeded reactions, NM<sup>R2E2</sup> showed a significantly shorter lag time than NM<sup>wt</sup>, indicating a faster rate of spontaneous confor-

mational conversion, whereas in such reactions NM<sup>AR2-5</sup> formed no fibers at all (Fig. 5d).

#### Biological implications

One common behavior of several amyloidogenic peptides is the conversion of their soluble structures into ordered, self-propagating aggregates. In some amyloidogenic polypeptides that are normally unstructured, osmolytes and elevated temperatures induce a gain of structure; this promotes conformational conversion<sup>15-19</sup>. In contrast, structured proteins and PrP<sup>sen</sup>, the protease-sensitive conformer of PrP, have to be partially unfolded — for example, with elevated temperature or chemical treatment — to achieve a convertible structural state. Stabilization of structure in their soluble forms is counterproductive to conformational conversion<sup>12,13,23-25</sup>.

Our results suggest the biological importance of the naturally existing structural flexibility of NM for  $[PSI^+]$  inheritance. They highlight the thin line between more stable structures that impede prion propagation, less stable structures that allow switching between nonprion ( $[psi^-]$ ) and prion ( $[PSI^+]$ ) states, and altered structures that increase the rates of spontaneous  $[psi^-]$  to  $[PSI^+]$  conversion. The prion-determining domain of Sup35p is highly conserved in different yeasts and, at least in some cases, the prion state  $[PSI^+]$  provides advantages for growth<sup>26,27</sup>. We propose that in the case of  $[PSI^+]$ , structural flexibility has been honed by evolutionary processes to provide stability in both the soluble and the aggregated state, creating stable but reversible protein-based phenotypes.

#### Methods

**Constructs and bacterial strains.** Using pEMBL-Sup35p (ref. 28) as a template for NM<sup>wt</sup>, pJLI-Sup35<sup>R2E2</sup> as a template for NM<sup>R2E2</sup> and pJLI-SUP35<sup>AR2-5</sup> as a template for NM<sup>AR2-5</sup>, DNA encoding NM<sup>wt</sup>, NM<sup>R2E2</sup> or NM<sup>AR2-5</sup>, respectively, was amplified by PCR. For recombinant expression, the PCR products were subcloned as *NdeI*-*Bam*HI fragments into pJC25. For GST-fusions, the PCR products for NM<sup>wt</sup> were subcloned as *Bam*HI-*Eco*RI fragments into pGEX-2T (Pharmacia). Proteins were expressed in *Escherichia coli*



# letters

BL21 [DE3] after induction with 1 mM IPTG ( $OD_{600nm}$  of 0.6) at 25 °C for 3 h.

**Protein purification.** NM<sup>wt</sup>, NM<sup>R2E2</sup> or NM<sup>AR2-5</sup> were purified after recombinant expression in *E. coli* as described for NM<sup>wt</sup> (ref. 29). GST-NM<sup>wt</sup> was purified using Glutathione-Sepharose (Boehringer Mannheim), Poros HQ (Boehringer Mannheim) and S-Sepharose (Pharmacia). The GST-NM fusion, linked with a thrombin cleavage site, was digested with thrombin, and GST was removed by binding to Glutathione-Sepharose. All purification steps for GST-NM<sup>wt</sup> were performed in the presence of 50 mM arginine-HCl. Protein concentrations were determined using the calculated extinction coefficient of 0.90 (NM<sup>wt</sup>), 0.69 (NM<sup>AR2-5</sup>), 1.00 (NM<sup>R2E2</sup>) and 1.23 (GST-NM<sup>wt</sup>) for a 1mg ml<sup>-1</sup> solution in a 1 cm cuvette at 280nm (ref. 30).

**Secondary structure analysis.** CD spectra were obtained using a Jasco 715 spectropolarimeter equipped with a temperature control unit. All spectra were taken with a 0.1 cm pathlength quartz cuvette (Hellma) in 5 mM potassium phosphate, pH 7.4, and 150 mM NaCl (standard buffer) or respective additives as indicated. Thermal transitions were performed with a heating/cooling increment of 0.5 °C min<sup>-1</sup>. The mean residue ellipticities were recorded for 30 s at 208 nm and 222 nm for each temperature. Settings for wavelength scans were 5 nm bandwidth; 0.25 s response time; 20 nm min<sup>-1</sup>; and four accumulations.

**Curve fits.** All kinetic traces were fit by least square calculations using the Sigma Plot version 6.0 software (SPSS). Folding and unfolding kinetics were fit by a single exponential. CR binding kinetics were fit with sigmoidal curve fits.

**Congo red binding.** CR binding was carried out as described<sup>7</sup>. Proteins were diluted to a final concentration of 1 μM into standard buffer plus 10 μM Congo red and incubated for 1 min at 25 °C before measuring the absorbance at 540 nm and 477 nm.

**Light scattering.** Buffers and samples were filtered twice using Millex-GP 0.22 μM syringe filters (Millipore). Static light scattering was monitored with a Dawn DSP laser photometer (Wyatt). The laser wavelength was set to 632.8 nm and scattering was monitored at a 90° angle. Data were analyzed using Astra version 4.5 (Wyatt). Dynamic light scattering was monitored with a PD2000 laser photometer (Precision Detectors, Inc.). The laser wavelength was set to

800 nm and scattering was monitored at a 90° angle. Data were analyzed using Precision Deconvolve software, using a mass-normalization for a random coil protein (Precision Detectors, Inc.).

## Acknowledgments

This research was supported by the National Institutes of Health, the Howard Hughes Medical Institute, the Keck Foundation, the University of Chicago Materials Research Science and Engineering Center and a postdoctoral fellowship of the Deutsche Forschungsgemeinschaft (T.S.). We gratefully acknowledge A. Kowal for Electron Microscopy, G. Sawicki for Atomic Force Microscopy, J.-J. Liu and H.-C. Chang for sharing unpublished results, J. Frederikson and J. Rehm for experimental help, and J. Bloom, M. Duennwald, T.F. Outeiro and H. True-Knob for comments on the manuscript.

Correspondence should be addressed to S.L.L. *email: lindquist@wi.mit.edu*

Received 23 May, 2001; accepted 20 August, 2001.

1. Patino, M.M., Liu, J.J., Glover, J.R. & Lindquist, S.L. *Science* **273**, 622–626 (1996).
2. Paushkin, S.V., Kushnirov, V.V., Smirnov, V.N. & Ter-Avanesyan, M.D. *EMBO J.* **15**, 3127–3134 (1996).
3. Stansfield, I. *et al. EMBO J.* **14**, 4365–4373 (1995).
4. Wickham, R.B. *Science* **264**, 566–569 (1994).
5. Serio, T.R. & Lindquist, S.L. *Annu. Rev. Cell Dev. Biol.* **15**, 661–703 (1999).
6. Prusiner, S.B. & Scott, M.R. *Annu. Rev. Genet.* **31**, 139–175 (1997).
7. Glover, J.R. *et al. Cell* **89**, 811–819 (1997).
8. Serio, T.R. *et al. Science* **289**, 1317–1321 (2000).
9. DePace, A.H., Santoso, A., Hillner, P. & Weissman, J.S. *Cell* **93**, 1241–1252 (1998).
10. Klunk, W.E., Jacob, R.F. & Mason, R.P. *Methods Enzymol.* **309**, 285–305 (1999).
11. Esler, W.P. *et al. J. Struct. Biol.* **130**, 174–183 (2000).
12. Dobson, C.M. *Trends Biochem. Sci.* **24**, 329–332 (1999).
13. Kelly, J.W. *Curr. Opin. Struct. Biol.* **8**, 101–106 (1998).
14. Pain, R.H. *Symp. Soc. Exp. Biol.* **41**, 21–33 (1987).
15. Zhang, S. & Rich, A. *Proc. Natl. Acad. Sci. USA* **94**, 23–28 (1997).
16. Kaye, R. *et al. J. Mol. Biol.* **287**, 781–796 (1999).
17. Gursky, O. & Aleshkov, S. *Biochim. Biophys. Acta* **1476**, 93–102 (2000).
18. Ramirez-Alvarado, M., Merkel, J.S. & Regan, L. *Proc. Natl. Acad. Sci. USA* **97**, 8979–8984 (2000).
19. Yang, D.S., Yip, C.M., Huang, T.H., Chakrabarty, A. & Fraser, P.E. *J. Biol. Chem.* **274**, 32970–32974 (1999).
20. Tuite, M.F., Mundy, C.R. & Cox, B.S. *Genetics* **98**, 691–711 (1981).
21. Singer, M.A., Lindquist, S.L. *Mol. Cell* **1**, 639–648 (1998).
22. Liu, J.J. & Lindquist, S.L. *Nature* **400**, 573–576 (1999).
23. Wong, C. *et al. EMBO J.* **20**, 377–386 (2001).
24. Kocisko, D.A. *et al. Proc. Natl. Acad. Sci. USA* **92**, 3923–3927 (1995).
25. Tatzelt, J., Prusiner, S.B. & Welch, W.J. *EMBO J.* **15**, 6363–6373 (1996).
26. Eaglestone, S.S., Cox, B.S. & Tuite, M.F. *EMBO J.* **18**, 1974–1981 (1999).
27. True, H. & Lindquist, S.L. *Nature* **407**, 477–485 (2000).
28. Ter-Avanesyan, M.D. *et al. Mol. Microbiol.* **7**, 683–692 (1993).
29. Scheibel, T., Kowal, A., Bloom, J. & Lindquist, S.L. *Curr. Biol.* **11**, 366–369 (2001).
30. Gill, S.C. & von Hippel, P.H. *Anal. Biochem.* **182**, 319–326 (1989).